ACS MATERIALS LETTERS

www.acsmaterialsletters.org

Weak Bonds, Strong Effects: Enhancing the Separation Performance of UiO-66 toward Chlorobenzenes via Halogen Bonding

Roman Gulyaev, Oleg Semyonov, Georgy V. Mamontov, Alexey A. Ivanov, Daniil M. Ivanov, Minjun Kim, Václav Svorčík, Giuseppe Resnati, Ting Liao, Ziqi Sun, Yusuke Yamauchi, Pavel S. Postnikov,* and Olga Guselnikova*

Cite This: *ACS Materials Lett.* 2023, 5, 1340−1349

Read Online

ACCESS | Metrics & More | Article Recommendations | Supporting Information

ABSTRACT: **Halogen bonding (HaB) is a weak interaction that assists in the recognition of nucleophilic molecules. However, HaB elements are currently under-investigated as a part of functional materials in separation science. Herein, we develop a novel approach for introducing HaB elements into UiO-66 to fine-tune the adsorption properties toward chlorobenzenes (CBs). A series of UiO-66 containing various contents of 2-iodoterephtalic acid (I-TA) (0%, 33%, 50%, 67%, and 100%) was prepared, characterized, and applied for the selective removal of CB contaminants from nonchlorinated aromatic analogues that cannot be separated by common distillation. Investigation of the structure−property relationship revealed that the highest adsorption capacity was achieved in the case of UiO-66 loaded with 50% I-TA (UiO-66-I_{opt}), and this was attributed to the balance between the number of HaB elements and the surface area of the UiO-66 structure. According to density functional theory calculations, the formation of a conjugate between dichlorobenzene and UiO-66-I_{opt} was more energetically favorable (up to 1.7 kcal/mol) than that of the corresponding conjugate with UiO-66. The formation of HaBs was experimentally verified by UV−vis, Raman, and X-ray photoelectron spectroscopies. To obtain functional materials for separation applications, waste polyethylene terephthalate (PET) was used as a support and feedstock for the surface-assisted growth of UiO-66-I_{opt}. The as-prepared PET@UiO-66-I_{opt} exhibited a close-to-perfect selectivity and reusability for the separation of a wide range of CBs from nonchlorinated aromatic analogues.**

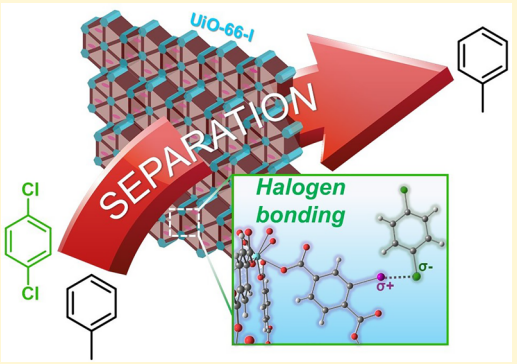

Intermolecular interactions play a significant role in all processes in which molecular recognition and self-assembly occur. They are of crucial importance in nanoscience, nanotechnology, and other fields as diverse as catalysis,[1a] biopharmacology,[1b] and photophysics.[1c] Optimization of the interactional landscape in a material is therefore essential to boost its functional performance in target applications.[1]

The halogen bond (HaB) is an attractive interaction in which a halogen atom acts as the electrophilic site.[2a] This type of interaction is a relatively new entry in the toolbox available to scientists for controlling the structural and functional properties of systems in the gas, liquid, and solid phases.[2] To date, HaBs have been successfully employed in the synthesis of molecular[3] and polymeric[4a] materials such as liquid crystals,[4b] gels,[4c] and photoluminescent compounds.[4d] They have also been extensively used to improve the properties of bioactive derivatives, more specifically to promote the binding of a drug to a receptor[5] and enhancing the processability of a solid active principle.[6] In addition, halogen bonded systems have been employed as pure substances or composites for the molecular recognition and binding of neutral molecules,[7] ions,[8] and ion pairs[9] in the solution or gas phases.[4b] The potential of HaBs has also been explored in the capture of substances of environmental concerns,[10] such as in the removal of radioactive diiodine[10a] and the extraction of perfluoroalkyl iodides.[10b] However, despite its rapidly evolving applications in molecular recognition, halogen bonding is currently under-investigated[10c] in the context of functional materials for use in separation science.

Received: December 12, 2022
Accepted: March 20, 2023
Published: April 3, 2023

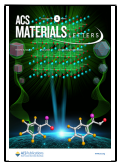

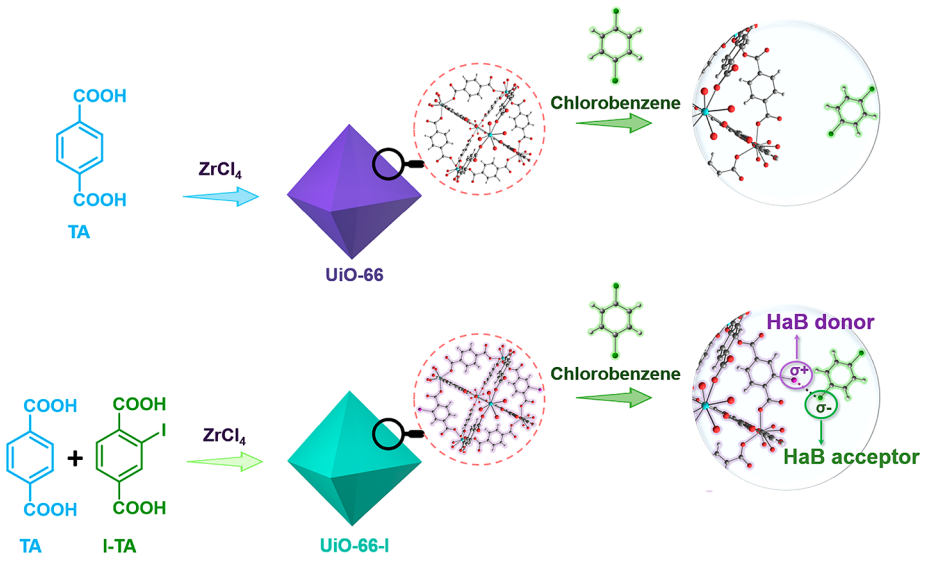

Figure 1. Artwork picturing the binding of 1,4-dichlorobenzene (DCB, a prototypal CB) by UiO-66-I via the HaB-based I···Cl supramolecular synthon. The reported UiO-66-I structure is that of UiO-66 (CSD refcode AZALOF) wherein one iodine atom has been "electronically" substituted for a hydrogen atom.

One possible solution for enhancing the usage of HaBs for separation is the hybridization of halogen-bonded systems with metal−organic frameworks (MOFs). Although MOFs are well-known functional materials for gas separation,[11] their application in the separation of structurally similar molecules in the liquid phase is also gaining momentum.[11c]

The tailored functionalization of MOFs is a useful synthetic strategy for tuning the recognition and binding of guest species.[12−14] For instance, di-, tri-, and tetracarboxylic acids (e.g., biphenyl and *p*-terphenyl 4,4′-dicarboxylic acids,[12b,13a] trimesic acid,[13b] and pyromellitic acids[12c,13c]) substituted with halogen atoms and bearing functionalities based on oxygen, nitrogen, sulfur, or other elements have been employed as organic ligands between metal nodes. As the selectivity of MOFs toward chlorobenzenes (CBs) primarily originates from the decorating groups present in the framework, the functionalization of organic linkers is generally considered to optimize the separation properties. For example, Zr-based MOFs, including UiO-66 and UiO-67, are widely used as templates to introduce additional functionalities.[12c,14]

More specifically, the high surface area, enhanced chemical and thermal stabilities, and exceptional tunability of UiO-66 allow its versatile use in a range of applications.[13c] UiO-66-based adsorbents have previously been demonstrated to exhibit good efficiencies in the removal of dyes,[15] insecticides,[16] and metal ions;[17] hence, it was expected that the UiO-66 framework might also be applicable for the adsorption and selective separation of CB derivatives as target pollutants. The separation of benzene derivatives is known to be both energy intensive and laborious because of their similar physicochemical properties.[18] From the perspective of environmental safety, the selective removal of CB contaminants from aquatic environments is, therefore, of great interest. Although nonchlorinated contaminants can be safely disposed of by incineration,[18a] this process is not suitable for chloroarenes due to the possible formation of dangerous phosgenes or chlorine oxides.[18a]

In this study, iodine-functionalized UiO-66 (UiO-66-I) is initially prepared by incorporating 2-iodoterephthalic acid (I-TA) as the linker. The as-prepared UiO-66-I is then employed for the adsorption of CBs and its activity is compared to that of the pristine UiO-66. It is hypothesized that UiO-66-I will exhibit a higher adsorption capacity due to the presence of iodine atoms that can act as HaB donor elements. The formation of HaBs between UiO-66-I and the CBs is experimentally and theoretically investigated using Raman and X-ray photoelectron spectroscopies, and density functional theory (DFT) calculations. Subsequently, to demonstrate the applicability of the developed materials, waste polyethylene terephthalate (PET) is employed as a support for the surface-assisted growth of UiO-66-I and the feedstock of terephthalic acids. Finally, the adsorption capacity and selectivity of the prepared PET@UiO-66-I toward CBs in the presence of nonchlorinated aromatic analogues.

Although CBs are widely used in the chemical and pharmaceutical industries, they present numerous health concerns because of their acute toxicity, bioaccumulation, suspected endocrine toxicity, immunotoxicity, and neurotoxicity.[16a,19] In addition, owing to their persistence, groundwater contamination by CBs is a serious environmental hazard.[17] CBs can function both as HaB donors via the small regions of depleted electron density opposite to the C−Cl covalent bond (σ-holes) and as HaB acceptors via the more extended belt region orthogonal to the C−Cl bonds. The limited size of the σ-holes at the Cl atoms imposes severe structural requirements for achieving the structural directionality and orientation required for effective HaB formation with chlorine acting as the HaB donor atom. Moreover, the surface electrostatic potential at the halogen σ-holes is weakly positive (e.g., $V_{S,max}$ = 5.3 kcal/mol for chlorobenzene[20a]), which is related to the known tendency of unfunctionalized CBs to function as weak HaB donors. In contrast, the negative belt occupies a significantly larger area of the molecule, and its negative electrostatic potential enables it to effectively interact with sites exhibiting a positive electrostatic potential, thereby serving as a HaB acceptor.[20b] It was therefore considered that the HaB-assisted adsorption and selective separation of CBs using functionalized UiO-66 frameworks could be enhanced by exploiting the negative belts of the chlorine atoms by installing HaB donor sites on the MOF surfaces. Thus, for this purpose,

https://doi.org/10.1021/acsmaterialslett.2c01169
ACS Materials Lett. 2023, 5, 1340−1349

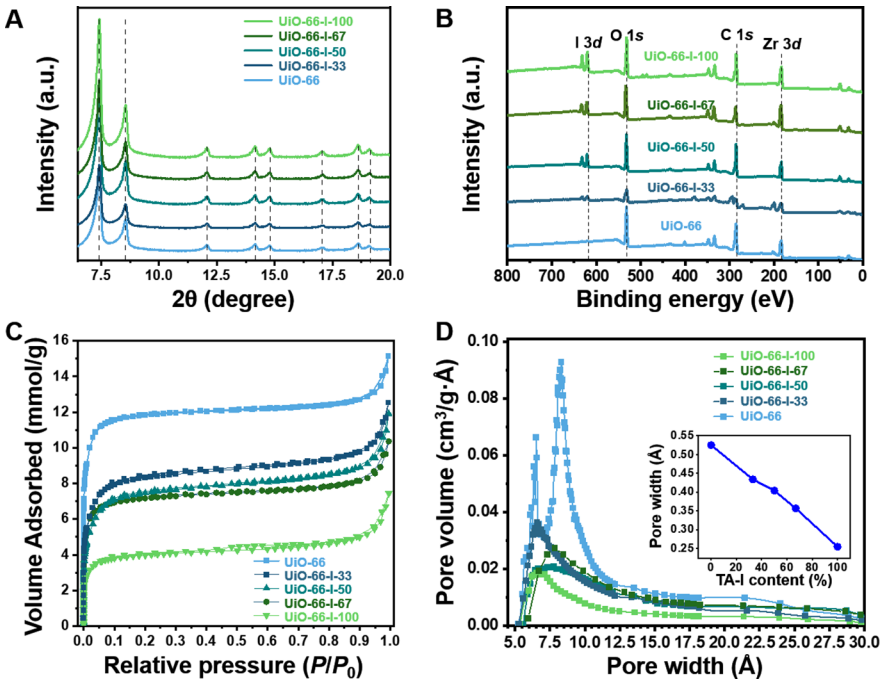

Figure 2. Characterization of UiO-66-I-*X* (*X* = 0−100): (A) XRD patterns, (B) XPS survey spectra, (C) nitrogen sorption isotherms, and (D) pore size distribution curves obtained by the Horváth−Kawazoe (HK) model.

iodine atoms were introduced to UiO-66 in the form of I-TA that was used as a type of organic linker along with TA (Figure 1). Iodine is preferred over other halogens because it is the strongest HaB donor (i.e., HaB donor ability: F < Cl < Br < I).[20c]

Functionalized UiO-66 samples containing varying ratios of I-TA and TA (I-TA/TA = 0%, 33%, 50%, 67%, and 100%) were prepared and denoted as UiO-66-I-*X* (where *X* indicates the percentage of I-TA). The formation of MOF mixed ligands is known to proceed in different ways depending on the ligand ratios employed.[21] Thus, to determine the I-TA contents of the prepared MOFs, quantitative analysis was performed for both the TA and I-TA ligands in UiO-66 by means of digestion and ^{1}H nuclear magnetic resonance (NMR) spectroscopic analysis of the disassembled frameworks in an appropriate medium (Figure S1). Analysis of the obtained data confirmed that the ligand ratio was comparable to the target ratio in the I-TA/TA mixture (Table S1).

Subsequently, the as-prepared UiO-66-I-*X* (*X* = 0−100) species were characterized by powder X-ray diffraction (XRD), revealing the expected peaks at 7.3, 8.5, 12, 14.1, 14.8, and 17°.[21,22] The XRD patterns of UiO-66-I-33, UiO-66-I-50, UiO-66-I-67, and UiO-66-I-100 matched those of pristine UiO-66 (Figure 2A), confirming that the mixed-ligand framework of UiO-66-I-*X* is isostructural with a face-centered cubic (FCC) structure. In addition, the Fourier transform infrared (FTIR) spectrum of UiO-66 features sharp bands at 1663, 1583, and 1395 cm^{-1} corresponding to the coordinated carboxyl groups and the asymmetric and symmetric stretches of the COO—Zr bonds, respectively (Figure S2A and Table S2). The FTIR spectra of UiO-66-I-50 and UiO-66-I-100 show additional bands at 760 cm^{-1} (C—I stretching vibrations) and 1470 cm^{-1} (C-CAr vibrations) associated with the presence of additional substituent in the aromatic ring (Figure S2B and Table S2). X-ray photoelectron spectroscopy (XPS) was also used to study the elemental compositions of the prepared MOFs and verify the presence of I-TA. As a result, the survey XPS spectra (Figure 2B) confirm a gradual increase in the iodine content from 1.7 to 4.6 atom % upon increasing the I-TA loading (Table S3).

As shown in Figure S3, the XPS spectra for Zr 3d are deconvoluted into two components at ∼185.3 eV (Zr 3d$_{3/2}$) and ∼182.9 eV (Zr 3d$_{5/2}$); this is in good agreement with previously published results.[15] The I 3d spectra confirm the appearance of I-TA units, with the typical I 3d doublets being observed at 632.9 and 621.3 eV (Figure S4).[23a] The additional low-intensity components at ∼630.9 and ∼618.9 eV confirm the presence of lower-coordinate ligands owing to defects in UiO-66-I-*X*, as reported previously.[23b]

The nitrogen sorption isotherms of the samples measured at 77 K are shown in Figure 2C. All samples exhibited microporous nature of the mixed-ligand Zr-MOFs. UiO-66 was found to exhibit a typical surface area of 1068 m^2/g (Table S4), and the introduction of I-TA led to a gradual decrease in surface area and pore volume. The surface areas for UiO-66-I-33, UiO-66-I-50, UiO-66-I-67, UiO-66-I-100 are 743, 660, 637, and 350 m^2/g, respectively. As expected, the bulky I atoms (atomic radius = 0.14 nm) occupy some of the space in the framework, as observed previously for a similar mixed-ligand system.[21] To obtain detailed information regarding the porosity and pore architecture of UiO-66-I, the pore size distributions of the specimens were plotted according to the Horváth−Kawazoe (HK) model (suitable for microporous materials, Figure 2D).[24a] The observed peaks at 0.65 and 0.83 nm correspond to the tetrahedral and octahedral pores of a nondefective UiO-66 framework.[24b] The introduction of I-TA causes a decrease in the volume of tetrahedral pores and an increase in octahedral-related pores, which was attributed to missing linker (ML) defects.[21,24c] The absence of mesopores indicates that there is only a negligible level of defect originating from the missing clusters. In contrast to the decrease in the internal pore volume of UiO-66 after

https://doi.org/10.1021/acsmaterialslett.2c01169
ACS Materials Lett. 2023, 5, 1340−1349

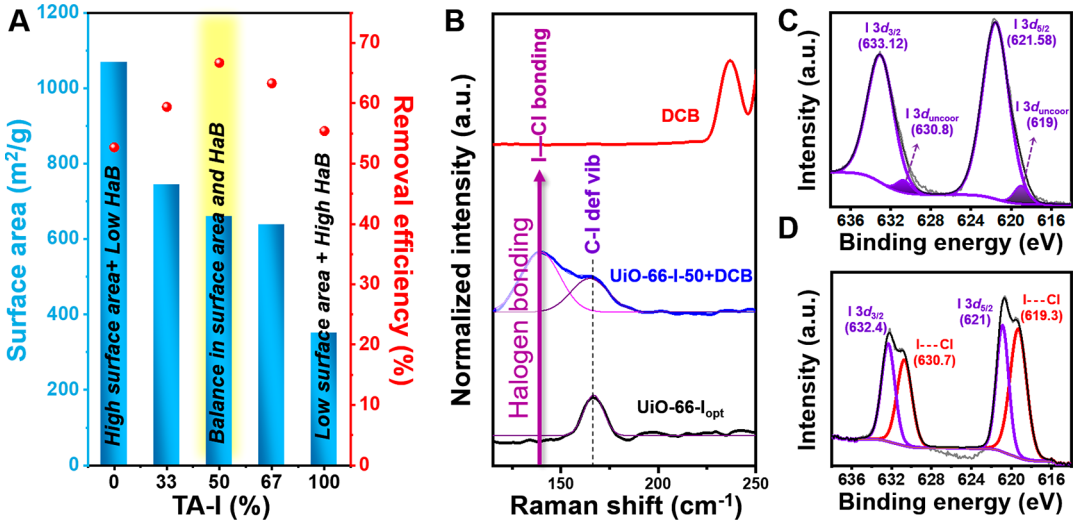

Figure 3. (A) DCB removal efficiency vs I-TA loading amount in UiO-66-I-*X*. The figure shows the balance between these parameters to achieve the maximum removal efficiency of DCB (150 μM) using 5 mg of the UiO-66-I-*X* (*X* = 0−100)adsorbent. (B) Low-frequency region of the Raman spectra of DCB and UiO-66-I$_{opt}$ before and after interaction with the DCB solution. XPS I 3d region for UiO-66-I$_{opt}$ (C) before and (D) after interaction with the DCB solution.

introducing I-TA to the framework, the presence of ML defects potentially have the opposite effect by increasing the internal pore volume. Thus, to verify the presence of ML defects, the procedure described by Lillerud et al.[24d] was employed (Figure S5A). More specifically, the thermogravimetric (TG) analysis (Figure S5) shows that an increase in the I-TA content of UiO-66-I from 0% to 100% results in a decrease in the number of carboxylate units per cluster from 12 to 6.9, indicating that up to 40 wt % of UiO-66-I-*X* (*X* = 0−100) consists of ligand defects. These changes correlate with the broadened Zr 3d (Figure S3) peaks, indicating that modification of the active center coordination environment may take place in the presence of ML defects.[24d] In general, an increase in the I content in the UiO-66-I frameworks has contrary effects on the possible CB adsorption and binding process. When the I-TA content is increased, the number of HaB donor sites available for CB binding via I···Cl HaBs is increased, and the number of ML defects in the structure is also increased (as proven by TG, XPS, and pore size distribution). In addition, the surface area and pore volume are reduced, indicating that the size effect of the bulky I atom prevails over the effect of the ML defects (Table S4).

Prior to evaluating the effect of the I-TA content on the adsorption of CBs, the possible formation of I···Cl HaBs was theoretically evaluated. For this purpose, DFT calculations were performed using a single-molecule model based on I-TA and 1,4-dichlorobenzene (DCB, Figure S6). The theoretical study reveals the possibility of forming a HaB between DCB as a nucleophile and I-TA as a σ-hole source with considerable strength (from −1.6 to −2.0 kcal/mol). Moreover, the initial results of single-molecule modeling were confirmed by periodic DFT calculations using models of UiO-66 and UiO-66-I-50 clusters (Figures S7−S10). The formation of a conjugate between DCB and UiO-66-I$_{opt}$ was found to be more energetically favorable (up to 1.7 kcal/mol) than the conjugate with UiO-66 (Table S5). The difference is in accordance with the corresponding I···Cl HaB energies.

To experimentally reveal the complex influence of I-TA loading on the adsorption properties of UiO-66-I, an in-depth analysis was conducted for the adsorption capacities (Figure S11) and the removal efficiencies of DCB by UiO-66-I-*X* (*X* = 33%, 50%, 67%, and 100%, Figure 3A). It was identified that UiO-66 is capable of removing 52% of the DCB from an aqueous solution (150 μM, 1000 mL), while UiO-66-I-33 and UiO-66-I-50 exhibit improved adsorption efficiencies of 60% and 67%, respectively.

Interestingly, further increases in the I-TA content (i.e., for UiO-66-I-67 and UiO-66-I-100) result in a reduction in the adsorption capacity toward DCB. It therefore demonstrates that the reduced surface area by the increased content of I-TA, in turn, negatively affects the adsorption performance. However, because the I atoms present in UiO-66-I-*X* are responsible for the formation of HaBs, which are required for the generation of selective interactions with CB, a careful balance between the surface area and the number of HaB elements is required to maximize the removal efficiency of CB. As UiO-66-50 offers the optimized adsorption performance, it is denoted as UiO-66-I$_{opt}$ in the following discussion.

Importantly, these effects offer a considerable advantage in terms of the material cost effectiveness because the price of UiO-66-I$_{opt}$ is 50% cheaper than that of UiO-66-I-100 (Table S6). Owing to its high removal efficiency, UiO-66-I$_{opt}$ was selected to experimentally confirm the formation of I···Cl HaBs, as suggested by theoretical calculations. The first indication of possible HaB formation was given by the UV−vis spectra (Figure S12), wherein the peak at 194 nm for UiO-66-I$_{opt}$ was blue-shifted by ∼3 nm after exposure to the DCB solution.[25a] According to IUPAC rules,[2a] the UV−vis absorption bands of the HaB donor usually shift to shorter wavelengths; thus, it can be used to detect the formation of HaBs. However, the observed blue shifts are less noticeable than those revealed by XPS and Raman spectroscopy. Indeed, Raman spectroscopy has been previously employed to monitor the C−I stretching band at ∼150−300 cm^{-1},[25a−d] which shifts to lower energies (or forms a new peak) during I···X bonding.[25a] Upon exposure to DCB, the Raman spectrum of UiO-66-I$_{opt}$ undergoes minor changes (Figure S13 and Table S7) that are similar to those observed for other HaB systems,[25b−d] and the most relevant variations are observed for modes associated with the C−I bond. More specifically, the

https://doi.org/10.1021/acsmaterialslett.2c01169
ACS Materials Lett. 2023, 5, 1340−1349

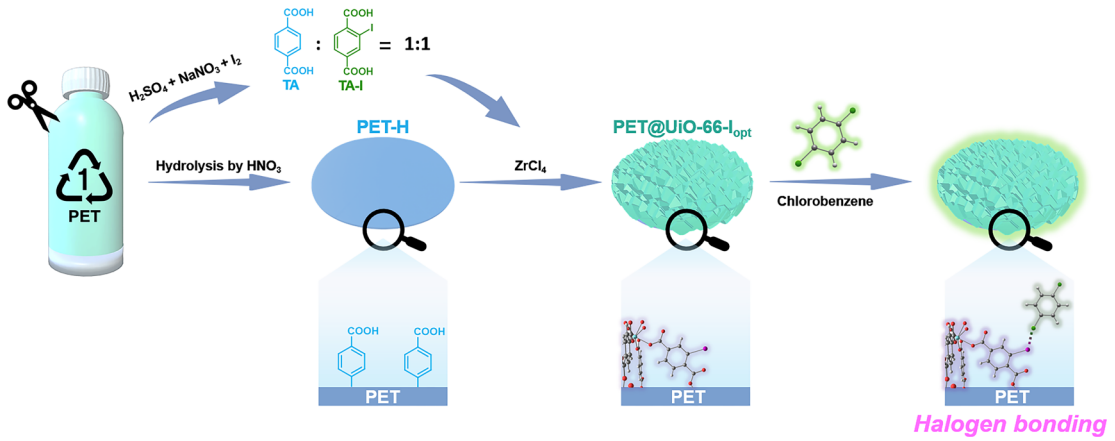

Figure 4. Preparation of PET@UiO-66-I_{opt} from waste PET and its application in the adsorption of CBs.

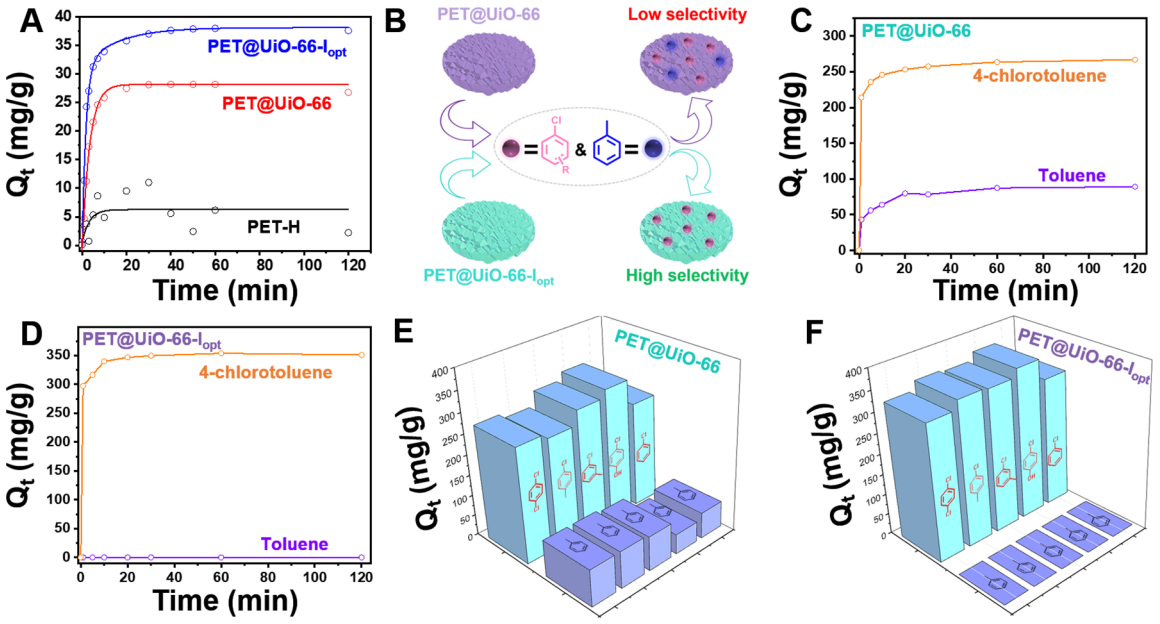

Figure 5. (A) Comparison of the adsorption capacities of hydrolyzed PET chips, PET@UiO-66, and PET@UiO-66-I_{opt} (5 mg) toward DCB (15 μM). (B) Schematic representation of the experimental strategy for evaluating the selectivity of CB removal over toluene. Adsorption kinetics of a 1:1 mixture of toluene/4-chlorotoluene (150 μM) on (C) PET@UiO-66 and (D) PET@UiO-66-I_{opt}. Comparison of the adsorption capacities (Q_e) of (E) PET@UiO-66 and (F) PET@UiO-66-I_{opt} of a solution containing toluene and 150 μM of various CBs (i.e., 1,4-dichlorobenzene, 4-chlorotoluene, 3-chlorotoluene, 4-chlorophenol, and chlorobenzene) in competitive adsorption experiments.

peak at 164 cm^{-1} (C−I deformation vibrations) shifts to 138 cm^{-1} (Figure 3B), which is consistent with I···Cl HaB formation between the DCB and I-TA ligands.

XPS analysis of the I 3d spectra of UiO-66-I_{opt} shows a slight downshift in the positions of the 630.8, 633.1, 621.6, and 619.0 eV peaks after DCB exposure (Figure 3C). These changes after HaB formation have also been reported in other relevant systems whose HaBs involve the I atom as a σ-hole donor.[23,25] As indicated in Figure 3D, the observed downshift is attributed to the electron density at the I atom being elevated upon HaB formation. Overall, the UV−vis, Raman, and XPS analyses confirm that the Cl atoms of DCB are halogen-bonded to the I atoms of I-TA in the porous structure of UiO-66-I_{opt}.

To understand the adsorption mechanism associated with UiO-66-I, the pore size distributions before and after DCB exposure were investigated. Typically, the volume of micropores of UiO-66 (centered at 0.65 and 0.83 nm) is relatively reduced in the presence of DCB, while the pore volumes in the mesopore region remain rather consistent (Figure S14A). This suggests that the nonfunctionalized and high-surface-area pristine UiO-66 adsorbed DCB mainly in its micropores. In contrast, the adsorption of DCB causes a substantial decrease in the pore volume in both the micro- and mesopore regions of UiO-66-I_{opt} (Figure S14B). The loss of pore volume in the mesopore region suggests that the mesopores derived from ML defects in UiO-66-I_{opt} (Figure S5) are more actively involved in the adsorption of DCB than the micropores, which underlines the importance of the morphology in the adsorption of DCB.

Following the above optimization studies, the practical and scalable use of UiO-66-I_{opt} as an effective adsorbent for CBs was investigated (Figure 4). The application of MOFs in their powder form is generally hampered by their low wettability and permeability, which render them less appealing and attractive in practical scenarios.[15a,b] Herein, the surface-assisted growth of UiO-66 on a PET support was adopted as an

https://doi.org/10.1021/acsmaterialslett.2c01169
ACS Materials Lett. 2023, 5, 1340−1349

effective strategy to overcome this issue.[15] Importantly, the use of PET waste as feedstock decreases the cost of the materials associated with this system. Indeed, the possibility of employing waste PET as a source of ligands for MOF construction has attracted significant research interest in terms of the development of functional upcycling methods.[15,26]

For UiO-66-I_{opt} growth on PET, a mixture of I-TA/TA ligands was synthesized by the Tronov–Novikov method[27] using PET waste as a feedstock (Figures S15 and S16). The prepared PET@UiO-66-I_{opt} material was fully characterized using FTIR, XRD, XPS, BET, and scanning electron microscopy combined with energy dispersive spectroscopy (SEM-EDX), as described in the Supporting Information (Figures S17–S22 and Table S8). Based on the obtained results, it is confirmed that a homogeneous polycrystalline film of UiO-66-I_{opt} was formed, and its properties are similar to those of UiO-66-I_{opt}. Importantly, the preparation of UiO-66-I_{opt} from cheap and available waste PET reduces the estimated cost associated with the material (Table S9).

The PET@UiO-66-I_{opt} material should exhibit adsorption properties similar to those of the pure UiO-66-I_{opt}, but PET-supported materials are preferable for separation application.[15a,b] Thus, the prepared PET@UiO-66-I_{opt} was tested in the selective removal of CBs in the presence of nonhalogenated arenes from aqueous solutions. To verify the key role of HaBs in this process, the adsorption of diluted DCB (15 μM, 100 mL) was compared on PET-H, PET@UiO-66, and PET@UiO-66-I_{opt} as a function of the contact time 23 °C (Figure 5A). PET-H demonstrates a low adsorption capacity with a considerable disorder of the DCB concentration over time, indicating the reversibility of DCB capture. In contrast, PET@UiO-66 achieves more efficient adsorption with an adsorption capacity (Q_e) of 28.2 mg/g, as calculated using eq 1:

$$Q_e = \left(\frac{(C_0 - C_e) \times M}{m}\right) \times V \quad (1)$$

where C_0 (μM) is the initial concentration of the DCB, C_e (μM) is the concentration of the solution at equilibrium, M is the molecular weight of DCB (147 g/mol), m (mg) is the mass of adsorbent employed, and V (L) is the solution volume.

As shown in Figure 5A, PET@UiO-66-I_{opt} exhibits a 30% increase in adsorption capacity as compared to PET@UiO-66, potentially due to the presence of HaB donor elements. The adsorption of DCB into the pores of PET@UiO-66-I_{opt} occurs rapidly, with 87% of the DCB being removed from the aqueous solution only after 20 min. Beyond this point, the adsorption rate decreases until reaching the equilibrium at ∼40 min. This short equilibration time can be attributed to the uniform pores present in the polycrystalline film and the ease of access of the HaB elements.[28] This improved adsorption capacity, therefore, allows more efficient and potentially selective separation of CBs from the mixtures involving nonhalogenated aromatic compounds.

Separation processes are essential technologies in nearly every aspect of any chemical industrial process.[11] The selective separation of chlorinated aromatics is more challenging than their simple sorption, particularly when the selectivity is significantly compromised among structurally similar aromatic molecules.[11b] As mentioned above, although the different disposal routes required by chloroarenes and arenes necessitate their separation,[18] previously reported materials did not provide high adsorption capacities or selectivities for the separation of chloroarenes over their nonhalogenated analogues (Table S10). Thus, the separation abilities of PET@UiO-66 and PET@UiO-66-I_{opt} were tested using aqueous solutions (150 μM, 100 mL) containing toluene and a mixture of CBs (i.e., 1,4-dichlorobenzene, 4-chlorotoluene, 3-chlorotoluene, and 4-chlorophenol).

A kinetic study was then carried out for the adsorption of a mixture of toluene and 4-chlorotoluene using PET@UiO-66 and PET@UiO-66-I_{opt}. As shown in Figure 5B, these two adsorbents exhibit drastically different behaviors. More specifically, for PET@UiO-66, both toluene and 4-chlorotoluene are taken into the pores (Figure 5C), while for PET@UiO-66-I_{opt}, only 4-chlorotoluene is adsorbed (Figure 5D). A similar tendency is observed for other mixtures (Figures S23 and S24), with PET@UiO-66 demonstrating a relatively low selectivity for different CBs in comparison with toluene (Figure 5E). It is therefore considered that the preferable capture of CBs be related to the Lewis basicity of chlorine, which may suggest a nonminor contribution of Lewis acid–base interactions to the adsorption phenomenon.[29] In contrast to previously reported materials (Table S10), PET@UiO-66-I_{opt} demonstrates an extremely high adsorption selectivity for the CBs over toluene (Figure 5F). Considering the lower surface area of PET@UiO-66-I_{opt} (surface area of powdery UiO-66-I-50, 660 m^2/g) compared to that of PET@UiO-66 (surface area of powdery UiO-66-I, 1068 m^2/g), it is reasonable to suggest that the exceptional selectivity correlates with the formation of HaBs between the electrophilic iodine (electropositive σ-holes) and the nucleophilic chlorine (electronegative belt). Despite the weakness of this interaction (1.65 kcal/mol according to DFT calculations), it succeeds in securing the selective sorption of CBs in the presence of toluene.

It is subsequently deduced that the adsorption of DCB by PET@UiO-66-I_{opt} occurs according to the pseudo-second-order model (Figures S25 and S26 and Tables S11 and S12), which is dominated by chemical interactions. The adsorption capacity is therefore related to the number of available HaB elements, and so the sorption of DCB by PET@UiO-66-I_{opt} could be assisted by (i) π–π interactions between the benzene rings of the DCB molecules and the aromatic structure of UiO-66,[30a,24a] (ii) Lewis acid–base interactions between the framework Zr and the Cl atom of DCB,[30b] (iii) hydrogen bonding (e.g., μ_3–OH···π interactions),[30c,d] and (iv) a suitable pore architecture.[30e] However, due to the different adsorption behaviors exhibited by PET@UiO-66 and PET@UiO-66-I_{opt} (Figure 5A), it is apparent that π–π and Lewis acid–base interactions are not likely to be dominant, but the adsorption capacity is enhanced by the pore architecture, implying the existence of active HaB elements and a suitable surface area.[30f,g] These assumptions agree with the above-described adsorption performances of the powdery UiO-66-I-*X*'s (X = 0%, 33%, 50%, 67%, or 100%). Analysis of the different adsorption models (Figure S27 and Table S13) shows the strongest correlation with the Freundlich isotherm (Figure S27). This indicates that DCB sorption occurs through multilayers of UiO-66 with Lewis acid centers and I acting as HaB donors. The adsorption profile of PET@UiO-66-I_{opt}, therefore, prompted us to evaluate its selective separation of DCB in the presence of nonchlorinated arenes.

To obtain further information regarding the role of I atoms in arene adsorption by the MOFs, adsorption capacities (Figure S28) and the removal efficiencies (Figure 6A) of

https://doi.org/10.1021/acsmaterialslett.2c01169
ACS Materials Lett. 2023, 5, 1340–1349

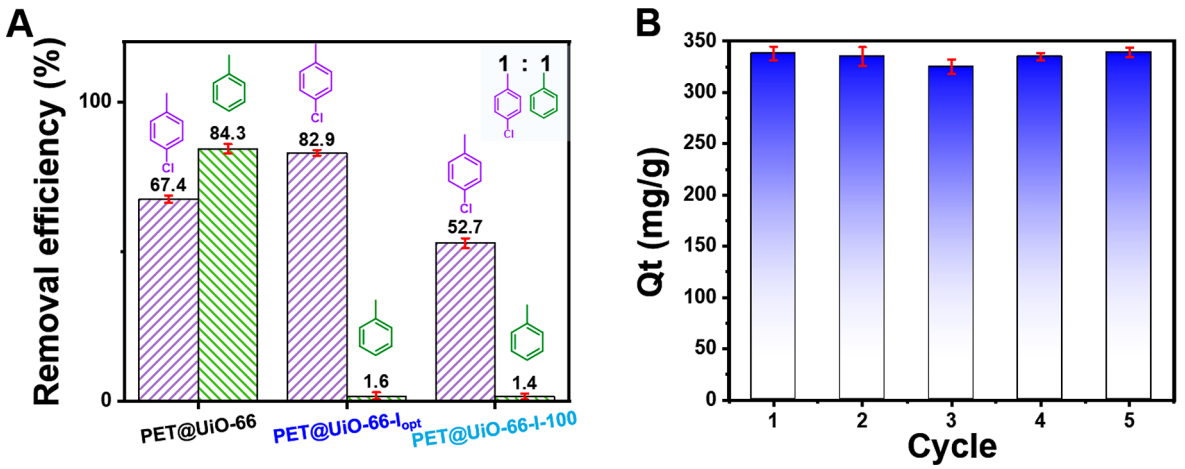

Figure 6. (A) Removal efficiencies of PET@UiO-66, PET@UiO-66-I$_{opt}$, and PET@UiO-66-I-100 for a 1:1 mixture of toluene/4-chlorotoluene (150 μM) (5 mg of each material). (B) Adsorption capacity of PET@UiO-66-I$_{opt}$ over five recycles.

PET@UiO-66, PET@UiO-66-I$_{opt}$, and PET@UiO-66-I-100 were compared using a 1:1 solution of toluene/4-chlorotoluene in water (150 μM, 100 mL). Interestingly, PET@UiO-66 adsorbs toluene with a preference over 4-chlorotoluene, which represents an opposite selectivity compared to the iodine-functionalized system, thereby confirming the active role of iodine in the CB adsorption process. PET@UiO-66-I-100 shows the same preferential adsorption of 4-chlorotoluene as PET@UiO-66-I$_{opt}$, but the selectivity is lower, possibly due to the lower surface area and/or increased number of defects in the fully iodinated system.

PET@UiO-66 adsorbed a greater amount of toluene than PET@UiO-66-I$_{opt}$ and PET@UiO-66-I-100, which preferentially adsorbed the CBs. At the same time, UiO-66 has the highest surface area compared to PET@UiO-66-I$_{opt}$ and PET@UiO-66-I-100 (Table S4). However, the Q_e of PET@UiO-66-I$_{opt}$ for 4-chlorotoluene is higher than those of PET@UiO-66 and PET@UiO-66-I-100 (Figure S28), thereby further demonstrating the importance of a balance between the material porosity and the number of HaB donor elements.

Finally, the possibility of recycling the PET@UiO-66-I$_{opt}$ adsorbent was evaluated after washing with ethanol and subsequent activation for 2 h at 60 °C. After five adsorption cycles in an aqueous DCB solution and subsequent desorption in ethanol, the sorption properties of PET@UiO-66-I$_{opt}$ remain largely unchanged (Figure 6B). This can be attributed to the conservation of its UiO-66-I$_{opt}$ crystal structure, as verified by XRD measurements (Figure S29).

In summary, this study demonstrates that the introduction of HaB elements into the structures of MOFs produces highly functional materials for the selective separation and removal of CB contaminants. The investigation of a series of UiO-66 MOFs with various contents of I-TA (i.e., 0%, 33%, 50%, 67%, and 100%) reveals that the highest adsorption capacity is achieved with a 50% I-TA content (UiO-66-I$_{opt}$), due to the fact that this composition leads to a balance between the surface area and the number of HaB recognition elements. The formation of halogen bonds between UiO-66-I$_{opt}$ and CBs is confirmed both theoretically and experimentally. HaBs have previously been used occasionally to assemble supramolecular organic frameworks by exploiting the established tendency of nitrogen-based HaB acceptors with iodobenzene derivatives or by exploiting the simultaneous action of HaBs and hydrogen bonds.[31] In addition, they have been used to enhance the functional properties of MOFs.[32] However, despite the diversity of previously reported structures that can utilize HaBs to drive the removal of halogenated contaminants (Table S14), achieving a high adsorption capacity and selectivity remained challenging. Thus, in the current study, the limitations of HaB use in separation science were challenged by improving the technological appeal of UiO-66-I$_{opt}$ containing HaB and decreasing the material cost. Within the framework of the suggested experimental strategy, waste PET was recycled for the surface-assisted growth of UiO-66-I$_{opt}$ using a mixture of TA and I-TA. The prepared PET@UiO-66-I$_{opt}$ exhibited a high adsorption capacity toward the CBs, which was described by the pseudo-second-order model, thereby confirming the role of the number of available HaB elements. This high adsorption capacity was accompanied by an unprecedented selectivity in the separation of CBs from nonchlorinated aromatic compounds owing to the formation of I···Cl HaBs. In addition, the prepared PET@UiO-66-I$_{opt}$ was successfully recycled five times without any loss in performance. These results suggest that high-surface-area MOFs operating in aqueous media and containing HaB donor or acceptor sites may be particularly promising for the sequestration of contaminants containing HaB acceptor or donor sites, respectively. It is anticipated that this work will lay the foundations for the use of HaB in the preparation of functional materials for contaminant separation.

■ ASSOCIATED CONTENT

Supporting Information

The Supporting Information is available free of charge at https://pubs.acs.org/doi/10.1021/acsmaterialslett.2c01169.

Prime cost calculations (XLSX)

Experimental details, PXRD, SEM, FTIR, BET, ^{1}H NMR, UV−vis, DFT calculations, Raman spectroscopy, TG, XPS, ICP-MC adsorption experiments, and recycling experiments (PDF)

■ AUTHOR INFORMATION

Corresponding Authors

Pavel S. Postnikov − *Research School of Chemistry and Applied Biomedical Sciences, Tomsk Polytechnic University, Tomsk 634050, Russian Federation; Department of Solid-*

https://doi.org/10.1021/acsmaterialslett.2c01169
ACS Materials Lett. 2023, 5, 1340−1349

State Engineering, University of Chemistry and Technology Prague, Prague 16628, Czech Republic; orcid.org/0000-0001-9713-1290; Email: postnikov@tpu.ru

Olga Guselnikova − *Research School of Chemistry and Applied Biomedical Sciences, Tomsk Polytechnic University, Tomsk 634050, Russian Federation; National Institute for Materials Science (NIMS), Tsukuba, Ibaraki 305-0044, Japan;* orcid.org/0000-0002-2594-9605; Email: guselnikovaoa@tpu.ru

Authors

Roman Gulyaev − *Research School of Chemistry and Applied Biomedical Sciences, Tomsk Polytechnic University, Tomsk 634050, Russian Federation*

Oleg Semyonov − *Research School of Chemistry and Applied Biomedical Sciences, Tomsk Polytechnic University, Tomsk 634050, Russian Federation;* orcid.org/0000-0002-9792-2006

Georgy V. Mamontov − *Tomsk State University, Tomsk 634050, Russian Federation*

Alexey A. Ivanov − *Research School of Chemistry and Applied Biomedical Sciences, Tomsk Polytechnic University, Tomsk 634050, Russian Federation*

Daniil M. Ivanov − *Research School of Chemistry and Applied Biomedical Sciences, Tomsk Polytechnic University, Tomsk 634050, Russian Federation; Institute of Chemistry, Saint Petersburg State University, Saint Petersburg 199034, Russian Federation*

Minjun Kim − *Australian Institute for Bioengineering and Nanotechnology (AIBN), The University of Queensland, Brisbane, Queensland 4072, Australia;* orcid.org/0000-0001-9962-6561

Václav Švorčík − *Department of Solid-State Engineering, University of Chemistry and Technology Prague, Prague 16628, Czech Republic*

Giuseppe Resnati − *Research School of Chemistry and Applied Biomedical Sciences, Tomsk Polytechnic University, Tomsk 634050, Russian Federation; NFMLab, Department of Chemistry, Materials and Chemical Engineering "Giulio Natta", Politecnico di Milano, I-20131 Milano, Italy;* orcid.org/0000-0002-0797-9296

Ting Liao − *School of Mechanical, Medical and Process Engineering, Queensland University of Technology, Brisbane, Queensland 4000, Australia;* orcid.org/0000-0001-7488-6244

Ziqi Sun − *School of Chemistry and Physics, Queensland University of Technology, Brisbane, Queensland 4000, Australia;* orcid.org/0000-0002-4777-4017

Yusuke Yamauchi − *Australian Institute for Bioengineering and Nanotechnology (AIBN), The University of Queensland, Brisbane, Queensland 4072, Australia; National Institute for Materials Science (NIMS), Tsukuba, Ibaraki 305-0044, Japan;* orcid.org/0000-0001-7854-927X

Complete contact information is available at: https://pubs.acs.org/10.1021/acsmaterialslett.2c01169

Author Contributions

CRediT: **Roman Gulyaev** data curation, formal analysis, investigation, methodology, writing-review & editing; **Oleg Semyonov** formal analysis, investigation, methodology, writing-original draft; **Grigory Vladimirovich Mamontov** data curation, formal analysis; **Alexey A. Ivanov** data curation, formal analysis; **Daniil M. Ivanov** data curation, formal analysis, investigation, writing-original draft; **Minjun Kim** software, visualization; **Václav Švorčík** data curation, formal analysis, funding acquisition, writing-review & editing; **Giuseppe Resnati** conceptualization, validation, writing-review & editing; **Ting Liao** data curation, formal analysis, investigation, methodology, software; **Ziqi Sun** resources, software; **Yusuke Yamauchi** resources, supervision, validation, writing-review & editing; **Pavel S. Postnikov** conceptualization, resources, supervision, writing-original draft, writing-review & editing; **Olga Guselnikova** conceptualization, investigation, project administration, supervision, visualization, writing-original draft, writing-review & editing.

Notes

The authors declare no competing financial interest.

■ ACKNOWLEDGMENTS

Support from the Ministry of Science and Higher Education of the Russian Federation in the framework of the "Mega-grant" project (No. 075-15-2021-585s) and GACR (GACR No. 22-02022S) is gratefully acknowledged. T.L. and Y.Y. acknowledge financial support from the Australian Research Council (FT160100281, DP200103568) and JST-ERATO, respectively. This research was also undertaken with the assistance of resources from the National Computational Infrastructure (NCI), which was supported by the Australian Government under the NCRIS program. The authors also thank the central laboratories of TPU (Analytical Center) for carrying out the XPS, XRD, and TGA measurements, and the Tomsk Regional Core Shared Research Facilities Centre of National Research Tomsk State University for carrying out the SEM and gas isotherm measurements. This work was performed in part at the Queensland node of the Australian National Fabrication Facility, a company established under the National Collaborative Research Infrastructure Strategy to provide nano- and microfabrication facilities for Australia's researchers.

■ REFERENCES

(1) (a) Neel, A. J.; Hilton, M. J.; Sigman, M. S.; Toste, F. D. Exploiting Non-Covalent π Interactions for Catalyst Design. *Nature* **2017**, *543*, 637−646. (b) Hutchins, K. M. Functional Materials Based on Molecules with Hydrogen-Bonding Ability: Applications to Drug Co-Crystals and Polymer Complexes. *R. Soc. Open Sci.* **2018**, *5*, 180564. (c) Qu, D.-H.; Wang, Q.-C.; Zhang, Q.-W.; Ma, X.; Tian, H. Photoresponsive Host−Guest Functional Systems. *Chem. Rev.* **2015**, *115*, 7543−7588.

(2) (a) Desiraju, G. R.; Ho, P. S.; Kloo, L.; Legon, A. C.; Marquardt, R.; Metrangolo, P.; Politzer, P.; Resnati, G.; Rissanen, K. Definition of the Halogen Bond (IUPAC Recommendations 2013). *Pure Appl. Chem.* **2013**, *85*, 1711−1713. (b) Turunen, L.; Hansen, J. H.; Erdélyi, M. Halogen Bonding: *An Odd Chemistry*. *Chem. Rec.* **2021**, *21*, 1252−1257. (c) Cavallo, G.; Metrangolo, P.; Milani, R.; Pilati, T.; Priimagi, A.; Resnati, G.; Terraneo, G. The Halogen Bond. *Chem. Rev.* **2016**, *116*, 2478−2601.

(3) (a) Priimagi, A.; Cavallo, G.; Metrangolo, P.; Resnati, G. The Halogen Bond in the Design of Functional Supramolecular Materials: *Recent Advances*. *Acc. Chem. Res.* **2013**, *46*, 2686−2695. (b) Berger, G.; Frangville, P.; Meyer, F. Halogen Bonding for Molecular Recognition: New Developments in Materials and Biological Sciences. *Chem. Commun.* **2020**, *56*, 4970−4981.

(4) (a) Vanderkooy, A.; Taylor, M. S. Solution-Phase Self-Assembly of Complementary Halogen Bonding Polymers. *J. Am. Chem. Soc.* **2015**, *137*, 5080−5086. (b) Wang, H.; Bisoyi, H. K.; Urbas, A. M.; Bunning, T. J.; Li, Q. The Halogen Bond: An Emerging Supramolecular Tool in the Design of Functional Mesomorphic Materials. *Chem. Eur. J.* **2019**, *25*, 1369−1378. (c) Meazza, L.; Foster, J. A.;

Fucke, K.; Metrangolo, P.; Resnati, G.; Steed, J. W. Halogen-Bonding-Triggered Supramolecular Gel Formation. *Nat. Chem.* **2013**, *5*, 42−47. (d) Zhu, W.; Zheng, R.; Zhen, Y.; Yu, Z.; Dong, H.; Fu, H.; Shi, Q.; Hu, W. Rational Design of Charge-Transfer Interactions in Halogen-Bonded Co-Crystals toward Versatile Solid-State Optoelectronics. *J. Am. Chem. Soc.* **2015**, *137*, 11038−11046.

(5) Hardegger, L. A.; Kuhn, B.; Spinnler, B.; Anselm, L.; Ecabert, R.; Stihle, M.; Gsell, B.; Thoma, R.; Diez, J.; Benz, J.; Plancher, J.; Hartmann, G.; Banner, D. W.; Haap, W.; Diederich, F. Systematic Investigation of Halogen Bonding in Protein−Ligand Interactions. *Angew. Chemie Int. Ed.* **2011**, *50*, 314−318.

(6) Baldrighi, M.; Cavallo, G.; Chierotti, M. R.; Gobetto, R.; Metrangolo, P.; Pilati, T.; Resnati, G.; Terraneo, G. Halogen Bonding and Pharmaceutical Cocrystals: The Case of a Widely Used Preservative. *Mol. Pharmaceutics* **2013**, *10*, 1760−1772.

(7) Metrangolo, P.; Carcenac, Y.; Lahtinen, M.; Pilati, T.; Rissanen, K.; Vij, A.; Resnati, G. Nonporous Organic Solids Capable of Dynamically Resolving Mixtures of Diiodoperfluoroalkanes. *Science* **2009**, *323*, 1461−1464.

(8) (a) Sarwar, M. G.; Dragisic, B.; Sagoo, S.; Taylor, M. S. A. Tridentate Halogen-Bonding Receptor for Tight Binding of Halide Anions. *Angew. Chemie Int. Ed.* **2010**, *49*, 1674−1677. (b) Chudzinski, M. G.; McClary, C. A.; Taylor, M. S. Anion Receptors Composed of Hydrogen- and Halogen-Bond Donor Groups: Modulating Selectivity With Combinations of Distinct Noncovalent Interactions. *J. Am. Chem. Soc.* **2011**, *133*, 10559−10567. (c) Mitchell, E. J.; Beecroft, A. J.; Martin, J.; Thompson, S.; Marques, I.; Félix, V.; Beer, P. D. Hydrosulfide (HS−) Recognition and Sensing in Water by Halogen Bonding Hosts. *Angew. Chemie Int. Ed.* **2021**, *60*, 24048−24053.

(9) Mele, A.; Metrangolo, P.; Neukirch, H.; Pilati, T.; Resnati, G. A Halogen-Bonding-Based Heteroditopic Receptor for Alkali Metal Halides. *J. Am. Chem. Soc.* **2005**, *127*, 14972−14973.

(10) (a) Yan, C.; Mu, T. Investigation of Ionic Liquids for Efficient Removal and Reliable Storage of Radioactive Iodine: A Halogen-Bonding Case. *Phys. Chem. Chem. Phys.* **2014**, *16*, 5071−5075. (b) Yan, X. Q.; Shen, Q. J.; Zhao, X. R.; Gao, H. Y.; Pang, X.; Jin, W. J. Halogen Bonding: A New Retention Mechanism for the Solid Phase Extraction of Perfluorinated Iodoalkanes. *Anal. Chim. Acta* **2012**, *753*, 48−56. (c) Peluso, P.; Mamane, V.; Dallocchio, R.; Dessì, A.; Villano, R.; Sanna, D.; Aubert, E.; Pale, P.; Cossu, S. Polysaccharide-Based Chiral Stationary Phases as Halogen Bond Acceptors: A Novel Strategy for Detection of Stereoselective σ-Hole Bonds in Solution. *J. Sep. Sci.* **2018**, *41*, 1247−1256.

(11) (a) Furukawa, H.; Cordova, K. E.; O'Keeffe, M.; Yaghi, O. M. The Chemistry and Applications of Metal−Organic Frameworks. *Science* **2013**, *341*, 6149. (b) Li, J.-R.; Sculley, J.; Zhou, H.-C. Metal−Organic Frameworks for Separations. *Chem. Rev.* **2012**, *112*, 869−932. (c) Nalaparaju, A.; Jiang, J. Metal−Organic Frameworks for Liquid Phase Applications. *Adv. Sci.* **2021**, *8*, 2003143. (d) Xie, L. H.; Liu, X. M.; He, T.; Li, J. R. Metal−Organic Frameworks for the Capture of Trace Aromatic Volatile Organic Compounds. *Chem.* **2018**, *4*, 1911−1927. (e) He, T.; Kong, X. J.; Bian, Z. X.; Zhang, Y. Z.; Si, G. R.; Xie, L. H.; Li, J. R. Trace Removal of Benzene Vapour using Double-walled Metal−Dipyrazolate Frameworks. *Nat. Mater.* **2022**, *21*, 689−695.

(12) (a) Li, J.; Wang, X.; Zhao, G.; Chen, C.; Chai, Z.; Alsaedi, A.; Hayat, T.; Wang, X. Metal−Organic Framework-Based Materials: Superior Adsorbents for the Capture of Toxic and Radioactive Metal Ions. *Chem. Soc. Rev.* **2018**, *47*, 2322−2356. (b) Islamoglu, T.; Chen, Z.; Wasson, M. C.; Buru, C. T.; Kirlikovali, K. O.; Afrin, U.; Mian, M. R.; Farha, O. K. Metal−Organic Frameworks against *Toxic Chemicals*. *Chem. Rev.* **2020**, *120*, 8130−8160. (c) Sudan, S.; Gładysiak, A.; Valizadeh, B.; Lee, J.-H.; Stylianou, K. C. Sustainable Capture of Aromatic Volatile Organic Compounds by a Pyrene-Based Metal−Organic Framework under Humid Conditions. *Inorg. Chem.* **2020**, *59*, 9029−9036. (d) Li, J.; Ye, W.; Chen, C. Removal of Toxic/Radioactive Metal Ions by Metal-Organic Framework-Based. *Materials* **2019**, *29*, 217−279. (e) Yu, F.; Bai, X.; Liang, M.; Ma, J. Recent Progress on Metal-Organic Framework-Derived Porous Carbon and Its Composite for Pollutant Adsorption from Liquid Phase. *Chem. Eng. J.* **2021**, *405*, 126960.

(13) (a) Wang, H.; Yu, L.; Lin, Y.; Peng, J.; Teat, S. J.; Williams, L. J.; Li, J. Adsorption of Fluorocarbons and Chlorocarbons by Highly Porous and Robust Fluorinated Zirconium Metal−Organic Frameworks. *Inorg. Chem.* **2020**, *59*, 4167−4171. (b) Krautwurst, J.; Smets, D.; Lamann, R.; Ruschewitz, U. How Does the Fluorination of the Linker Affect the Stability of Trimesate-Based Coordination Polymers and Metal−Organic Frameworks. *Inorg. Chem.* **2019**, *58*, 8622−8632. (c) Hayes, O. G.; Warrender, S. J.; Cordes, D. B.; Duncan, M. J.; Slawin, A. M. Z.; Morris, R. E. Preventing Undesirable Structure Flexibility in Pyromellitate Metal Organic Frameworks. *Eur. J. Inorg. Chem.* **2020**, *2020*, 2537−2544.

(14) (a) Islamoglu, T.; Ortuño, M. A.; Proussaloglou, E.; Howarth, A. J.; Vermeulen, N. A.; Atilgan, A.; Asiri, A. M.; Cramer, C. J.; Farha, O. K. Presence versus Proximity: The Role of Pendant Amines in the Catalytic Hydrolysis of a Nerve Agent Simulant. *Angew. Chemie Int. Ed.* **2018**, *57*, 1949−1953. (b) Katz, M. J.; Moon, S.-Y.; Mondloch, J. E.; Beyzavi, M. H.; Stephenson, C. J.; Hupp, J. T.; Farha, O. K. Exploiting Parameter Space in MOFs: A 20-Fold Enhancement of Phosphate-Ester Hydrolysis with UiO-66-NH_2. *Chem. Sci.* **2015**, *6*, 2286−2291. (c) Winarta, J.; Shan, B.; Mcintyre, S. M.; Ye, L.; Wang, C.; Liu, J.; Mu, B. A Decade of UiO-66 Research: A Historic Review of Dynamic Structure, Synthesis Mechanisms, and Characterization Techniques of an Archetypal Metal−Organic Framework. *Cryst. Growth Des.* **2020**, *20*, 1347−1362. (d) Chen, C.-X.; Wei, Z.-W.; Jiang, J.-J.; Zheng, S.-P.; Wang, H.-P.; Qiu, Q.-F.; Cao, C.-C.; Fenske, D.; Su, C.-Y. Dynamic Spacer Installation for Multirole Metal−Organic Frameworks: A New Direction toward Multifunctional MOFs Achieving Ultrahigh Methane Storage Working Capacity. *J. Am. Chem. Soc.* **2017**, *139*, 6034−6037.

(15) (a) Semyonov, O.; Chaemchuen, S.; Ivanov, A.; Verpoort, F.; Kolska, Z.; Syrtanov, M.; Svorcik, V.; Yusubov, M. S.; Lyutakov, O.; Guselnikova, O.; Postnikov, P. S. Smart Recycling of PET to Sorbents for Insecticides through in Situ MOF Growth. *Appl. Mater. Today* **2021**, *22*, 100910. (b) Semyonov, O.; Kogolev, D.; Mamontov, G.; Kolobova, E.; Trelin, A.; Yusubov, M. S.; Guselnikova, O.; Postnikov, P. S. Synergetic Effect of UiO-66 and Plasmonic AgNPs on PET Waste Support towards Degradation of Nerve Agent Simulant. *Chem. Eng. J.* **2022**, *431*, 133450. (c) Leus, K.; Perez, J. P. H.; Folens, K.; Meledina, M.; Van Tendeloo, G.; Du Laing, G.; Van Der Voort, P. UiO-66-$(SH)_2$ as Stable, Selective and Regenerable Adsorbent for the Removal of Mercury from Water under Environmentally-Relevant Conditions. *Faraday Discuss.* **2017**, *201*, 145−161.

(16) (a) Grimalt, J. O.; Sunyer, J.; Moreno, V.; Amaral, O. C.; Sala, M.; Rosell, A.; Anto, J. M.; Albaiges, J. Risk Excess of Soft-Tissue Sarcoma and Thyroid Cancer in a Community Exposed to Airborne Organochlorinated Compound Mixtures with a High Hexachlorobenzene Content. *Int. J. Cancer* **1994**, *56*, 200−203. (b) Trivedi, M. K.; Branton, A.; Trivedi, D.; Nayak, G.; Singh, R.; Jana, S. Physical, Thermal and Spectroscopic Studies on Biofield Treated p-Dichlorobenzene. *Biochem. Anal. Biochem.* **2015**, *4*, 1000204.

(17) Amaral, O. C.; Otero, R.; Grimalt, J. O.; Albaiges, J. Volatile and Semi-Volatile Organochlorine Compounds in Tap and Riverine Waters in the Area of Influence of a Chlorinated Organic Solvent *Factory*. *Water Res.* **1996**, *30*, 1876−1884.

(18) (a) Bonner, T. A.; Cornett, C. L.; Desai, B. O.; Fullenkamp, J. M.; Hughes, T. W. *Engineering Handbook for Hazardous Waste Incineration, Final report March−September*; Office of Scientific and Technical Information, 1981. (b) Zhang, G.; Emwas, A. H.; Shahul Hameed, U. F.; Arold, S. T.; Yang, P.; Chen, A.; Xiang, J. F.; Khashab, N. M. Shape-Induced Selective Separation of Ortho-Substituted Benzene Isomers Enabled by Cucurbit[7]Uril Host Macrocycles. *Chem.* **2020**, *6*, 1082−1096.

(19) Heidrich, S.; Schirmer, M.; Weiss, H.; Wycisk, P.; Grossmann, J.; Kaschl, A. Regionally Contaminated Aquifers? Toxicological Relevance and Remediation Options (Bitterfeld Case Study). *Toxicology.* **2004**, *205*, 143−155.

https://doi.org/10.1021/acsmaterialslett.2c01169
ACS Materials Lett. 2023, 5, 1340−1349

(20) (a) Riley, K. E.; Murray, J. S.; Fanfrlík, J.; Řezáč, J.; Solá, R. J.; Concha, M. C.; Ramos, F. M.; Politzer, P. Halogen Bond Tunability I: The Effects of Aromatic Fluorine Substitution on the Strengths of Halogen-Bonding Interactions Involving Chlorine, Bromine, and Iodine. *J. Mol. Model.* **2011**, *17*, 3309−3318. (b) Metrangolo, P.; Resnati, G. Metal-Bound Halogen Atoms in Crystal Engineering. *Chem. Commun.* **2013**, *49*, 1783−1785. (c) Terraneo, G.; Resnati, G.; Metrangolo, P. Iodine and Halogen Bonding. In *Iodine Chemistry and Applications*; John Wiley & Sons, Inc: Hoboken, NJ, 2014; pp 159−194.
(21) Chavan, S. M.; Shearer, G. C.; Svelle, S.; Olsbye, U.; Bonino, F.; Ethiraj, J.; Lillerud, K. P.; Bordiga, S. Synthesis and Characterization of Amine-Functionalized Mixed-Ligand Metal−Organic Frameworks of UiO-66 Topology. *Inorg. Chem.* **2014**, *53*, 9509−9515.
(22) Kalaj, M.; Momeni, M. R.; Bentz, K. C.; Barcus, K. S.; Palomba, J. M.; Paesani, F.; Cohen, S. M. Halogen Bonding in UiO-66 Frameworks Promotes Superior Chemical Warfare Agent Simulant *Degradation*. *Chem. Commun.* **2019**, *55*, 3481−3484.
(23) (a) Wang, F.; Ma, N.; Chen, Q.; Wang, W.; Wang, L. Halogen Bonding as a New Driving Force for Layer-by-Layer Assembly. *Langmuir* **2007**, *23* (19), 9540−9542. (b) Moreton, J. C.; Low, J. X.; Penticoff, K. C.; Cohen, S. M.; Benz, L. An X-Ray Photoelectron Spectroscopy Study of Postsynthetic Exchange in UiO-66. *Langmuir* **2022**, *38*, 1589−1599.
(24) (a) Rege, S. U.; Yang, R. T. Corrected Horváth-Kawazoe Equations for Pore-Size Distribution. *AIChE J.* **2000**, *46*, 734−750. (b) Ramsahye, N. A.; Gao, J.; Jobic, H.; Llewellyn, P. L.; Yang, Q.; Wiersum, A. D.; Koza, M. M.; Guillerm, V.; Serre, C.; Zhong, C. L.; Maurin, G. Adsorption and Diffusion of Light Hydrocarbons in UiO-66(Zr): A Combination of Experimental and Modeling Tools. *J. Phys. Chem. C* **2014**, *118*, 27470−27482. (c) Zhao, Y.; Zhang, Q.; Li, Y.; Zhang, R.; Lu, G. Large-scale Synthesis of Monodisperse UiO-66 Crystals with Tunable Sizes and Missing Linker Defects via Acid/Base Co-Modulation. *ACS Appl. Mater. Interfaces* **2017**, *9*, 15079−15085. (d) Shearer, G. C.; Chavan, S.; Ethiraj, J.; Vitillo, J. G.; Svelle, S.; Olsbye, U.; Lamberti, C.; Bordiga, S.; Lillerud, K. P. Tuned to Perfection: Ironing Out the Defects in Metal−Organic Framework UiO-66. *Chem. Mater.* **2014**, *26*, 4068−4071.
(25) (a) González, L.; Gimeno, N.; Tejedor, R. M.; Polo, V.; Ros, M. B.; Uriel, S.; Serrano, J. L. Halogen-Bonding Complexes Based on Bis(Iodoethynyl)Benzene Units: A New Versatile Route to Supramolecular Materials. *Chem. Mater.* **2013**, *25*, 4503−4510. (b) Tang, Y.; Huang, H.; Li, J.; Xue, W.; Zhong, C. IL-Induced Formation of Dynamic Complex Iodide Anions in IL@MOF Composites for Efficient Iodine Capture. *J. Mater. Chem. A* **2019**, *7*, 18324−18329. (c) Nagels, N.; Hauchecorne, D.; Herrebout, W. Exploring the C-X. . .π Halogen Bonding Motif: An Infrared and Raman Study of the Complexes of CF_3X (X = Cl, Br and I) with the Aromatic Model Compounds Benzene and Toluene. *Molecules.* **2013**, *18*, 6829−6851. (d) Klaeboe, P. The Raman Spectra of Some Iodine, Bromine, and Iodine Monochloride Charge-Transfer Coomplexes in Solution. *J. Am. Chem. Soc.* **1967**, *89*, 3667−3676.
(26) Shanmugam, M.; Chuaicham, C.; Augustin, A.; Sagayaraj, P. J.; Sasaki, K.; Sekar, K. Upcycling of Hazardous Metals and PET Waste derived Metal−Organic Frameworks: A Review in Recent Progress and Prospects. *New J. Chem.* **2022**, *46*, 15776−15794.
(27) Merkushev, E. V. Advances in the Synthesis of Aromatic Iodo-Compounds. *Russ. Chem. Rev.* **1984**, *53*, 343−350.
(28) Gao, Y.; Liu, K.; Kang, R.; Xia, J.; Yu, G.; Deng, S. A Comparative Study of Rigid and Flexible MOFs for the Adsorption of Pharmaceuticals: Kinetics, Isotherms and Mechanisms. *J. Hazard. Mater.* **2018**, *359*, 248−257.
(29) Caratelli, C.; Hajek, J.; Cirujano, F. G.; Waroquier, M.; Llabrés i Xamena, F. X.; Van Speybroeck, V. Nature of Active Sites on UiO-66 and Beneficial Influence of Water in the Catalysis of Fischer Esterification. *J. Catal.* **2017**, *352*, 401−414.
(30) (a) Zhao, W.; Zhang, C.; Yan, Z.; Zhou, Y.; Li, J.; Xie, Y.; Bai, L.; Jiang, L.; Li, F. Preparation, Characterization, and Performance Evaluation of UiO-66 Analogues as Stationary Phase in HPLC for the Separation of Substituted Benzenes and Polycyclic Aromatic Hydrocarbons. *PLoS One* **2017**, *12*, No. e0178513. (b) Zhuang, S.; Cheng, R.; Wang, J. Adsorption of Diclofenac from Aqueous Solution Using UiO-66-Type Metal-Organic Frameworks. *Chem. Eng. J.* **2019**, *359*, 354−362. (c) Chakarova, K.; Strauss, I.; Mihaylov, M.; Drenchev, N.; Hadjiivanov, K. Evolution of Acid and Basic Sites in UiO-66 and UiO-66-NH_2 Metal−Organic Frameworks: FTIR Study by Probe Molecules. *Microporous Mesoporous Mater.* **2019**, *281*, 110−122. (d) Grissom, T. G.; Sharp, C. H.; Usov, P. M.; Troya, D.; Morris, A. J.; Morris, J. R. Benzene, Toluene, and Xylene Transport through UiO-66: Diffusion Rates, Energetics, and the Role of Hydrogen Bonding. *J. Phys. Chem. C* **2018**, *122*, 16060−16069. (e) Lin, K.-Y. A.; Liu, Y.-T.; Chen, S.-Y. Adsorption of Fluoride to UiO-66-NH_2 in Water: Stability, Kinetic, Isotherm and Thermodynamic Studies. *J. Colloid Interface Sci.* **2016**, *461*, 79−87. (f) Molavi, H.; Zamani, M.; Aghajanzadeh, M.; Kheiri Manjili, H.; Danafar, H.; Shojaei, A. Evaluation of UiO-66 Metal Organic Framework as an Effective Sorbent for Curcumin's Overdose. *Appl. Organomet. Chem.* **2018**, *32*, No. e4221. (g) Ahmadijokani, F.; Molavi, H.; Rezakazemi, M.; Tajahmadi, S.; Bahi, A.; Ko, F.; Aminabhavi, T. M.; Li, J.-R.; Arjmand, M. UiO-66 Metal−Organic Frameworks in Water Treatment: A Critical Review. *Prog. Mater. Sci.* **2022**, *125*, 100904.
(31) Fan, Z.; Zou, Y.; Liu, C.; Xiang, S.; Zhang, Z. Hydrogen-Bonded Organic Frameworks: Functionalized Construction Strategy by Nitrogen-containing Functional Group. *Chem. Eur. J.* **2022**, *28*, No. e202200422.
(32) Martí-Rujas, J.; Colombo, L.; Lü, J.; Dey, A.; Terraneo, G.; Metrangolo, P.; Pilati, T.; Resnati, G. Hydrogen and Halogen Bonding Drive the Orthogonal Self-Assembly of an Organic Framework Possessing 2D Channels. *Chem. Commun.* **2012**, *48*, 8207−8209.

https://doi.org/10.1021/acsmaterialslett.2c01169
ACS Materials Lett. 2023, 5, 1340−1349